Journal of Power Sources 254 (2014) 48–54

Contents lists available at ScienceDirect

Journal of Power Sources

journal homepage: www.elsevier.com/locate/jpowsour

Insights into CO poisoning in high performance proton-conducting solid oxide fuel cells

Ning Yan, Xian-Zhu Fu, Karl T. Chuang, Jing-Li Luo*

Department of Chemical and Materials Engineering, University of Alberta, Edmonton, Alberta T6G 2G6, Canada

HIGHLIGHTS

- High performance anode supported PC-SOFC using BZCY electrolyte was fabricated.
- The presence of CO in fuel stream was able to deactivate Ni anode in PC-SOFC.
- Electrochemical reaction was evidenced to accelerate the poisoning process.

ARTICLE INFO

Article history:
Received 1 September 2013
Received in revised form
15 December 2013
Accepted 16 December 2013
Available online 22 December 2013

Keywords:
Proton-conducting solid oxide fuel cells
Syngas
CO poisoning
Carbon deposition

ABSTRACT

High performance anode supported proton-conducting solid oxide fuel cells (PC-SOFC) were fabricated and their performance in syngas was studied. PC-SOFC button cells produced a maximum power density of 812 mW cm^{-2} in H_2 at 750 °C. It was found that the CO-containing feed streams could drastically degrade the performance of PC-SOFC. Based on the experimental results and the theoretical analysis, the detailed process of the CO-induced Ni catalyst deactivation was identified. This process could be divided into three distinguishable stages during the continuous exposure of the Ni catalyst in the CO-containing environment. The first stage could be described using the CO surface active site blocking mechanism, which was further confirmed by CO/H_2 competitive adsorption model. The second stage deactivation was proposed to be related to the carbon deposition at TPB (Triple-phase Boundary). The deactivation during this stage was accelerated by the electrochemical conversion of H_2. The last stage was attributed to the coking of Ni catalyst and the resulted metal dusting effect.

1. Introduction

Solid oxide fuel cells with oxygen ion conducting electrolyte (OC-SOFC) have been intensively studied for the last several decades. OC-SOFC exhibits higher efficiency, lower environmental impact and comparable fuel diversity in comparison with the conventional thermal engine [1–3]. Since the discovery of protonic conductivity in some oxide materials in 1981 [4], many research efforts have been focused on the development of proton-conducting solid oxide fuel cell (PC-SOFC) including those fueled by hydrocarbons through internal steam reforming and/or water gas shift reaction [5–8]. The apparent advantage of PC-SOFC over OC-SOFC is its higher theoretical efficiency since the major electrochemical reaction product, H_2O, is generated at the cathode side without diluting the anode fuels.

In fact, the performance of PC-SOFC fed by fuels containing hydrocarbons is significantly lower than the theoretical value. Jamsak reported that the dramatic power density decrease of the PC-SOFC fed by ethanol was due to an increase in ohmic resistance [5]. The high temperature derivatives of ethanol are mainly CO, H_2 and CH_4. Ni et al., concluded that the extremely high ohmic overpotential and concentration overpotential were responsible for the poor performance of methane fueled PC-SOFC [6]. Luisetto conducted experiments with syngas (obtained by CH_4 internal CO_2-reforming) as the fuel for PC-SOFC and ascribed the low power density to carbon deposition and high reaction resistance [7]. Although Arpornwichanop speculated that CO might deteriorate PC-SOFC performance but the experimental evidence is needed to be more convincing [8]. In contrast to the strong CO surface active site blocking effect on metallic catalysts at low temperature in proton exchange membrane fuel cells (PEMFC) [9–11], CO chemisorption was greatly suppressed at high temperature during CO/H_2 competitive adsorption [12]. Thus, CO poisoning effect in PC-SOFC was not normally considered.

* Corresponding author. Tel.: +1 780 492 2232; fax: +1 780 492 2881.
E-mail address: Jingli.luo@ualberta.ca (J.-L. Luo).

0378-7753/$ – see front matter © 2013 Elsevier B.V. All rights reserved.
http://dx.doi.org/10.1016/j.jpowsour.2013.12.069

In this work, proton conductor $BaZr_{0.1}Ce_{0.7}Y_{0.2}O_{3-\delta}$ (BZCY) was used as the electrolyte when fabricating high performance anode supported PC-SOFC. The influence of CO on the performance of cells at 700 °C was studied and three distinguishable poisoning stages and corresponding mechanisms were proposed.

2. Experimental

2.1. Powder synthesis

Both BZCY electrolyte powder and $BaPrCo_2O_{6-\delta}$ (BPC) cathode material were synthesized through citrate–nitrate auto-combustion method: stoichiometric amounts of relevant metal nitrates were first dissolved in deionized water. Citric acid and NH_4NO_3 were then added to the solution as chelating agent and combustion fuel, respectively. The solution was magnetically stirred and heated with water evaporating. Finally, the solution residue was ignited and fine powder was formed by subsequent auto combustion. The as-prepared powder was then calcined at 1100 °C for 10 h in air to achieve a single phase oxide.

2.2. Anode supported button cell fabrication

A powder mixture of 33 wt% BZCY, 45 wt% NiO and 22 wt% corn starch was initially ball-milled in ethanol for 24 h. Then, the mixture was dried up and pressed into the pellets of 19 mm in diameter and ~800 μm in thickness. They were then pre-sintered at 1100 °C for 2 h to form strong anode substrate. The compositions of anode and cathode functional layers were 50 wt% BZCY + 50 wt% NiO and 50 wt% BZCY + 50 wt% BPC, respectively. These composite materials for the function layers were prepared through thorough mixing using ball mill.

Then NiO/BZCY anode functional layer and BZCY electrolyte were spin coated onto the strong substrate sequentially. The coated half-cell was then sintered at 1420 °C for 4 h for complete densification of the electrolyte. Finally, BPC/BZCY cathode layer was coated onto the dense electrolyte and then sintered at 1000 °C for 2 h. Before button cell test, diluted Ag paste was infiltrated into porous cathode layer in order to increase both activity and conductivity. The final active area of the fuel cell was 0.47 cm^2.

2.3. Characterization and electrochemical test

Both BZCY and BPC perovskite phases were identified using a Rigaku Rotaflex X-ray diffractometer (XRD) with Cu Kα radiation. The microstructures of anode supported button cells were characterized using a Hitachi S-2700 scanning electron microscope (SEM). The anode outlet gas composition was analyzed through gas chromatograph (GC, Agilent Technologies 6890N) when necessary. X-ray photoelectron spectroscopy (XPS) was performed using a Kratos Analytical AXIS 165.

In the fuel cell test, pure oxygen was used as the cathode oxidant with the flow rate of 50 mL min^{-1}. The anode inlet gas pressure was 137 kPa (20 psi) and its composition was adjusted using three independent and calibrated flow controllers connected to H_2, CO and N_2, respectively. Before electrochemical test, the membrane electrode assembly (MEA) was heated to selected operating temperature and then the anode component was reduced completely. During the test, impedance and current–voltage characteristics were determined in different gas mixtures using a Solartron 1287 electrochemical interface together with a 1255B frequency response analyzer. The impedance spectra of cells were obtained under open circuit with the AC amplitude of 10 mV and the frequency range from 0.1 Hz to 100 kHz.

3. Results and discussions

3.1. Button cell performances in H_2 and syngas

XRD patterns of BPC and BZCY in Fig. 1 confirm the pure perovskite phase without identifiable impurities. Fig. 2 shows the microstructure of the button cell cross-section. The BZCY electrolyte (~20 μm) was essentially dense without visible micro-pores or cracks. To investigate PC-SOFC performance, we examined the current–voltage characteristics and the corresponding power density curves in a stream of H_2. The button cell produced maximum power densities of 488 mW cm^{-2}, 592 mW cm^{-2}, 705 mW cm^{-2} and 812 mW cm^{-2} at 600 °C, 650 °C, 700 °C and 750 °C, respectively Fig. 3. The analysis of electrochemical impedance spectra is shown in Fig. 4, which confirms that the cell had a considerably low polarization resistance and therefore, was extremely sensitive to poisoning effect. The test temperature for PC-SOFC in syngas was selected to be at 700 °C since BZCY owns a high protonic transport number below this temperature [13,14]. Moreover, unfavorable side reactions between CO and H_2, such as methanation process, could be suppressed in this study when the temperature was above 700 °C. More details will be discussed in the following parts.

Fig. 5 compares the maximum power densities (MPD) of the PC-SOFC in three groups of feed streams at 700 °C. Since the MPD in CO containing fuels decreased as a function of exposure time, all the data were recorded after 30 min of treatment by the specified gases. In each individual group, the red arrow in the figure indicated the percentage of power density loss in CO containing feed relative to the corresponding CO free fuel. In group 1, the cells were fueled by either pure H_2 or pure CO. The MPD of 24 mW cm^{-2} was obtained in pure CO, which was 96.6% lower than that in H_2. It also implied that the BZCY electrolyte was not 100% protonic conductor at the testing temperature. The CO/H_2 ratio of syngas fuel in group 2 was fixed at 2, the same ratio as that of methane-derived syngas. Comparing with the cell fueled by the CO-free mixed gas of $N_2/H_2 = 2$, the MPD dropped 9.2% in syngas. The drop was extended to 34.4% in group 3 when the CO/H_2 ratio of syngas was raised to 9. (For interpretation of the references to colour in this figure legend, the reader is referred to the web version of this article.)

In the following sections, the negative effects of CO in the feed steam on the performance of PC-SOFC as a function of PC-SOFC

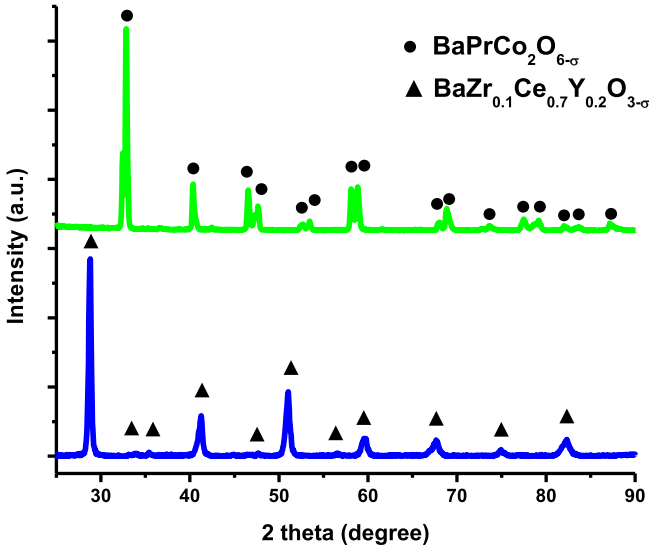

Fig. 1. XRD patterns of synthesized BPC and BZCY powders.

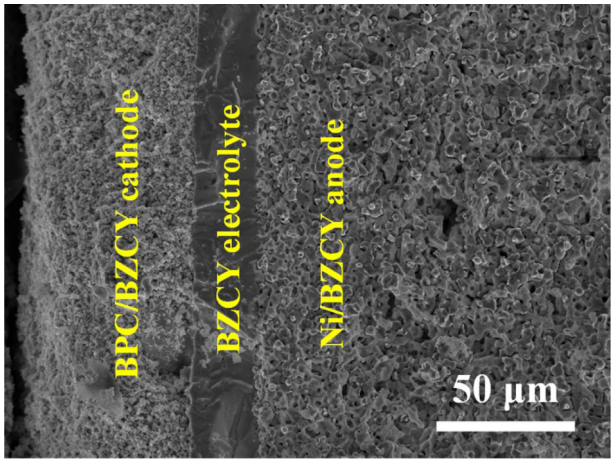

Fig. 2. SEM image of button cell cross-section after operation.

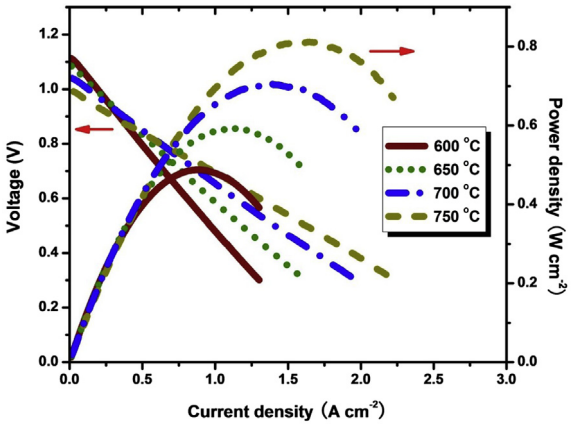

Fig. 3. I–V characteristics and power density curves in H_2 at different temperatures.

treatment time in syngas were systematically investigated. The H_2 concentration in syngas was fixed at 10% since lower H_2 content in the feedstock could drastically accelerate the poisoning rate leading to a more effective evaluation of the catalyst deactivation.

3.2. The 1st stage: chemical poisoning effect

The influence of CO on fuel cell performance was characterized through polarization curves and impedance spectra in 10% H_2 + CO. Around 20% of maximum power density loss was observed right after the balance gas was changed to CO from N_2 (Fig. 6), although the open circuit voltage (OCV) did not essentially change. All the ohmic resistances of the impedance spectra in Fig. 7 were not illustrated. After the balance gas was switched from N_2 to CO, an

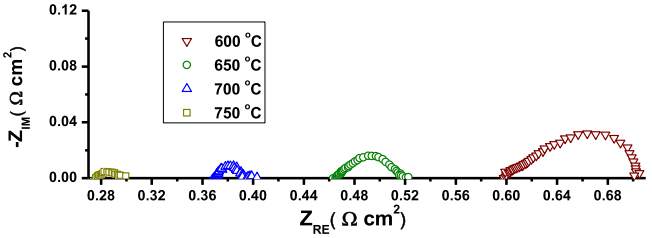

Fig. 4. Impedance spectra H_2 at different temperatures.

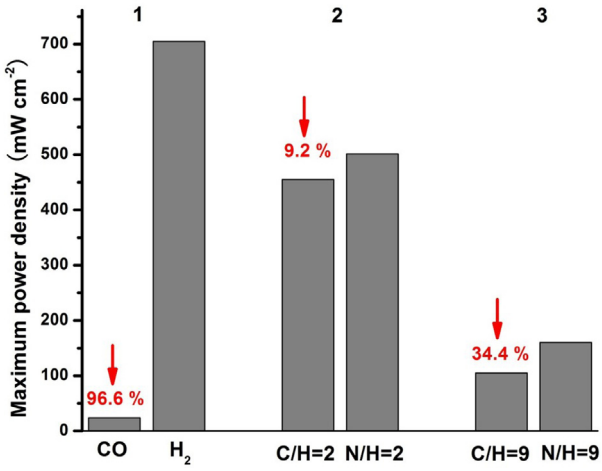

Fig. 5. A comparison of PC-SOFC maximum power densities in CO, H_2, syngas and N_2–H_2 gas mixtures at 700 °C.

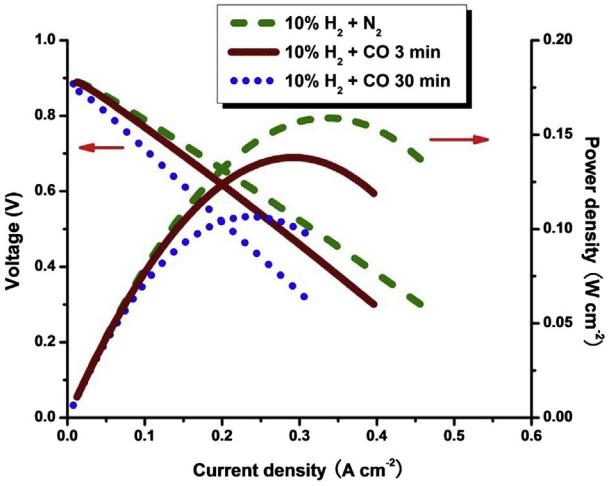

Fig. 6. A comparison of I–V characteristics and power density curves at different stages of CO poisoning at 700 °C.

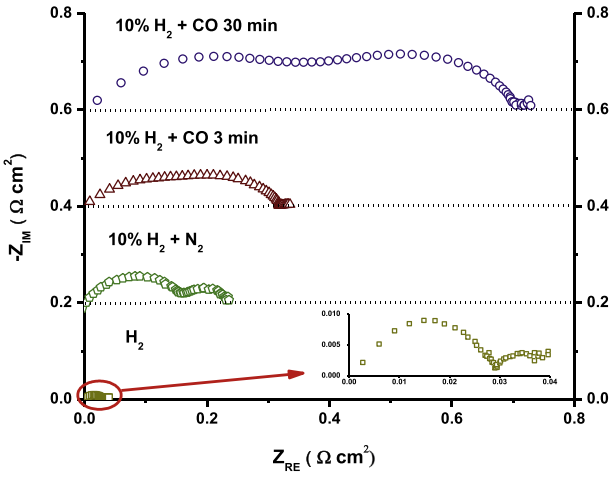

Fig. 7. A comparison of impedance spectra at different stages of CO poisoning at 700 °C.

increase in the polarization resistance was observed almost instantly. In the low frequency region, no pseudo-inductive response was observed in most of the CO poisoned PEMFC, implying that large CO coverage on the catalyst was unlikely to occur in PC-SOFC.

The CO poisoning effect was then evaluated under potentiostatic mode for a short period of time (Fig. 8). After initially introducing CO into the system, a sharp current drop immediately occurred. The magnitude of the drop was between 7% and 9%, depending upon the applied potentials. In addition, the variation of anode feed flow rate did not play a significant role in shaping the poisoning curves. Once CO was replaced by N_2 in the feed stream, the current started to recover and entirely returned to its original value after the substitution of anode chamber gas and the CO desorption from Ni were completed.

Since the binary diffusivities of H_2–N_2 and H_2–CO were essentially identical, the influence of fuel mass transport on PC-SOFC performance was negligible [15]. CO is not an inert gas as N_2, so it was readily activated by Ni catalyst. Since the chemisorbed CO molecules could not be oxidized in PC-SOFC, they might influence the activation as well as the conversion of H_2 molecules via either active site or geometric blocking mechanism. This could be part of the reason for the lower fuel cell performance and higher polarization resistance in syngas feed.

In order to evaluate the influence of CO on H_2 electrochemical oxidation in PC-SOFC at high temperature, a CO/H_2 competitive adsorption model was established. Both CO and H_2 adsorptions were based on Langmuir model as shown below,

$$H_2 + 2(Ni) \underset{k_d^H}{\overset{k_a^H}{\rightleftarrows}} 2H_{ad}(Ni) \quad (1)$$

$$CO + (Ni) \underset{k_d^{CO}}{\overset{k_a^{CO}}{\rightleftarrows}} CO_{ad}(Ni) \quad (2)$$

Where k_a and k_d represent the adsorption and the desorption rate constants, respectively; (Ni) indicates the surface active site on Ni. Assuming that the interaction among adsorbates was negligible and only linear structure of CO adsorption occurred [16], we can have the following expressions on surface coverage of CO (θ_{CO}) and H (θ_H) shown in (3) and (4).

$$\theta_H = \frac{\sqrt{\left(\frac{k_a^H P_{H_2}}{k_d^H}\right)}}{1 + \frac{k_a^{CO} P_{CO}}{k_d^{CO}} + \sqrt{\left(\frac{k_a^H P_{H_2}}{k_d^H}\right)}} \quad (3)$$

$$\theta_{CO} = \frac{\frac{k_a^{CO} P_{CO}}{k_d^{CO}}}{1 + \frac{k_a^{CO} P_{CO}}{k_d^{CO}} + \sqrt{\left(\frac{k_a^H P_{H_2}}{k_d^H}\right)}} \quad (4)$$

where P is the partial pressure of the specified gas. In the calculation, the total pressure was 137 kPa (same as the experimental condition). By using the kinetic parameters and equations derived from literature [17,18], θ_{CO} and θ_H were obtained as functions of temperature and H_2 partial pressure (Fig. 9).

In fact, CO molecule was able to bind with the transition metal catalyst much more strongly than H_2 as a result of its unique electronic band structure. For the competitive adsorption of CO and H_2 at low temperature (<200 °C), it is commonly known that the catalyst surface is exclusively covered by CO with surface coverage (θ_{CO}) being close to unity. The strong active site blocking effect was ascribed as the major reason for serious CO poisoning effect in PEMFC [9–11]. At high temperature (>600 °C), the adsorption of H_2 was not greatly affected by CO adsorption. Approximately 10% of the active sites were occupied by CO adsorbate in the syngas consisting of 10% H_2 + CO at 700 °C as calculated in Fig. 5. It was also logical to have observed 7–9% current drop when CO was introduced to the fuel in Fig. 8.

In summary, the instant degradations observed in Figs. 6–8 in syngas fuels could mainly be attributed to the active site blocking effect caused by the chemisorbed CO molecules on Ni.

3.3. The 2nd stage: electrochemical reaction accelerated carbon deposition

During the prolonged operation in CO containing feed, PC-SOFC performance gradually degraded as shown in Fig. 10. The maximum power density decreased to 60% of its original value and at the same time, a large increase of polarization resistance was detected, indicating severe deactivation of the catalyst and high degree of CO poisoning (Fig. 7). Nevertheless, little OCV drop occurred (Fig. 6) and the fuel cell ohmic resistance did not vary noticeably within this stage. The severe performance loss was still fully recoverable

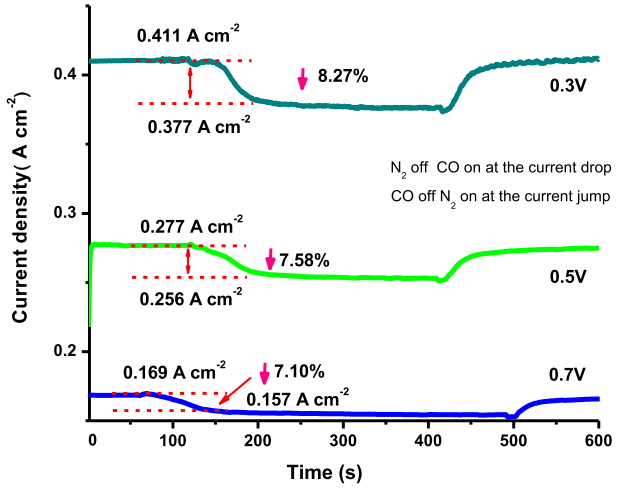

Fig. 8. Variations of current density with different applied voltages during the 1st stage of CO poisoning study under PC-SOFC potentiostatic mode at 700 °C.

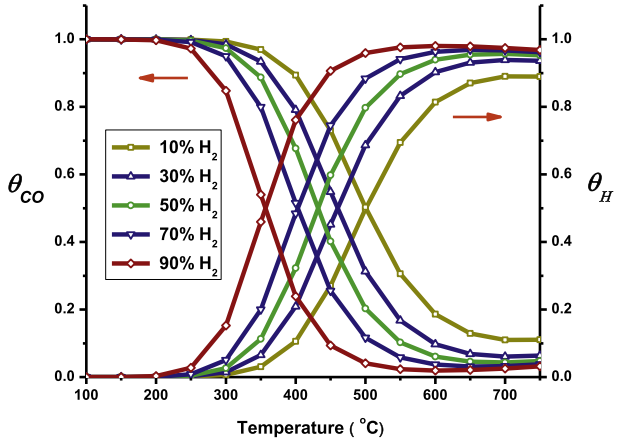

Fig. 9. H and CO surface coverage as functions of temperature and H_2 partial pressure with a total pressure was 137 kPa.

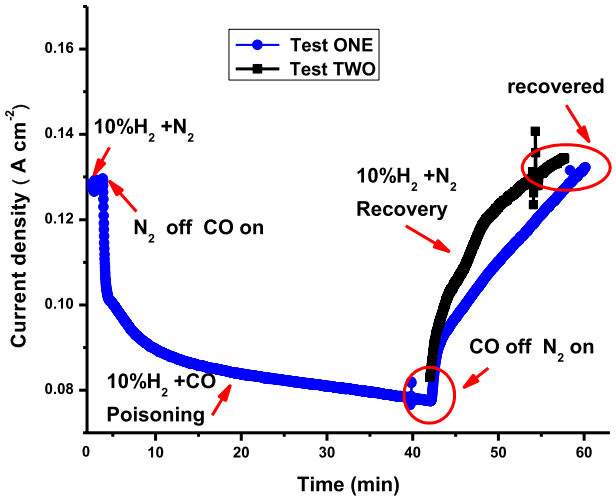

Fig. 10. CO poisoning and recovery in the 2nd stage under different testing conditions at 700 °C.

after CO flow was substituted by N_2. More importantly, we also found that the fuel cell operation conditions had an obvious influence on the extent of the performance degradation as shown in Fig. 10.

In an effort to find out the CO poisoning mechanisms in terms of chemical and electrochemical reaction effects, a pair of tests with identical CO treatment time was conducted. In test ONE, both CO poisoning and recovery process were recorded under potentiostatic mode at 0.75 V. As a contrast, in test TWO, the poisoning process was completed under OCV condition in which the PC-SOFC could be considered as a pure chemical reactor without any electrochemical reactions; the recovery was monitored under potentiostatic mode in order to determine and compare performance variations with test ONE. From the results shown in Fig. 10, it could be observed that in test ONE, the current density drop resulted from CO effect was more severe than that of test TWO. After the 1st stage poisoning, the current further decreased from 0.102 A cm^{-2} to 0.078 A cm^{-2} within 40 min in test ONE. However, after the identical time period of exposure to syngas, the performance only dropped to 0.082 A cm^{-2} in test TWO. During the recovery cycle, it took a longer time for the cell in test ONE to be fully recovered and a steeper curve for current density recovery was recorded in test TWO. As θ_{CO} was only ~10% under experimental conditions, it was no longer appropriate to reuse CO active site blocking mechanism to address the 2nd stage CO poisoning.

In fact, the SEM examinations showed little structure change of the anode in either cell after the CO poisoning experiments. Detailed surface information was revealed by the XPS analysis. Fig. 11 compares the spectra of C 1s for the cells operated in either test ONE or test TWO. The result indicates that carbon was deposited on the surface of Ni after syngas treatment. More importantly, a stronger carbon signal was always detected on the anode from test ONE.

When the fuel cell was a pure chemical reactor operated under OCV condition, the carbon deposition could be easily attributed to the applicable chemical reactions as below:

$$CO + H_2 \Leftrightarrow C + H_2O \quad (5)$$

$$2CO \Leftrightarrow C + CO_2 \quad (6)$$

Reaction (5) is kinetically much faster and thus became the major source of coke [19]. In contrast, when the fuel cell was working under potentiostatic mode, the case could become more complicated. In addition to the carbon sources from reaction (5) and (6), it was plausible that another parallel carbon source might start its contribution, or the existing carbon source was affected, possibly by the electrochemical oxidation of H_2. The overall effect accelerated the carbon deposition and caused more severe cell performance loss in test ONE.

Based on the above assumption from experimental data, we can propose an electrochemical reaction accelerated carbon deposition mechanism in explaining the 2nd stage CO poisoning. As soon as the electrochemical oxidation of H_2 started to proceed, a localized surface diffusion area (SDA) would be established adjacent to TPB and extended to Ni with a width of several hundreds of Angstrom [20]. When H_{ad} was electrochemically consumed at TPB, both H_{ad} and CO_{ad} located within SDA began to move and redistribute, driven by the gradient of chemical potential [20,21]. As the result of the dynamic equilibrium, θ_H tended to decrease whereas θ_{CO} to increase within SDA. Consequently, in comparison with a stand-by fuel cell functioning as a pure chemical reactor, higher θ_{CO} on Ni in an operating PC-SOFC led to a faster catalyzed carbon deposition rate and a slower rate of carbon removal. The larger amount of carbon deposits on the surface of Ni would block more active sites, further slowing down the H_2 electrochemical oxidation and more severely degrading PC-SOFC performance. Fig. 12 illustrates the schematic of the mechanism.

The 2nd stage CO poisoning started to reach equilibrium after 5 h of CO treatment and full reversibility was maintained (Fig. 13). Upon substitution of CO by N_2, there were basically two mechanisms which might be responsible for the carbon removal. The first one was the direct oxidation of carbon by oxygen since BZCY was not a pure proton conductor at the experimental temperature [13,14]. The PC-SOFC running in pure CO had a maximum power density of ~25 mW cm^{-2} as described in Fig. 5. The other mechanism could be explained by the reaction of the carbon with H_2 or water vapor derived from either the anode fuel stream or the residual product of reaction (5) (Fig. 14).

3.4. The 3rd stage: metal dusting of Ni

Fig. 13 shows a typical fuel cell destructive test when the operation potential was 0.75 V. A serious OCV drop was observed

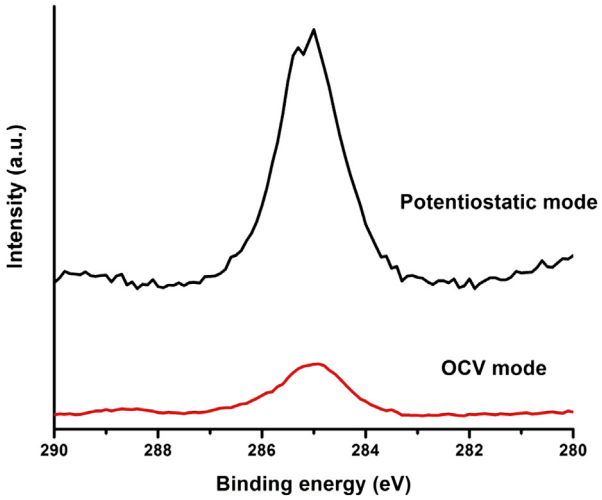

Fig. 11. XPS spectra of C1s obtained on PC-SOFC anode after tests in either potentiostatic mode or OCV mode.

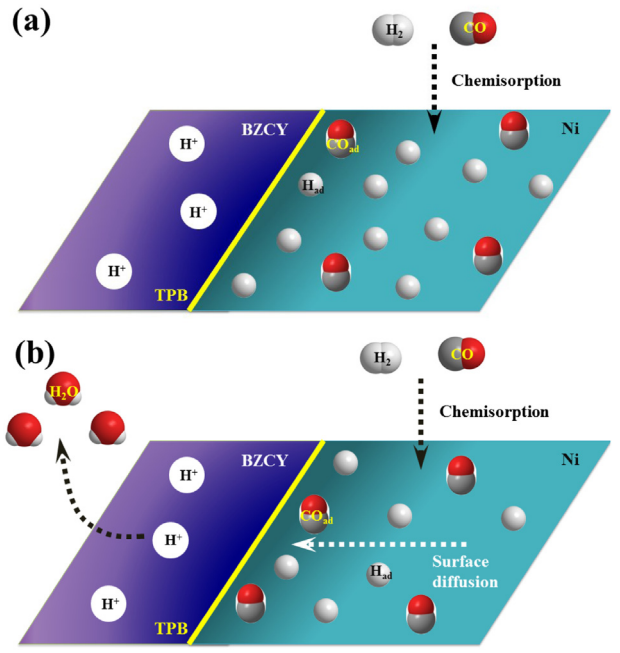

Fig. 12. Schematics of the electrochemical CO poisoning mechanism. (a) the original state of the adsorbate distribution within the TPB adjacent area in a stand-by PC-SOFC; (b) the equilibrium state of the adsorbate distribution within the TPB adjacent area in an operating PC-SOFC.

after 11 h of fuel cell operation in syngas. The main reason was believed to be the electrolyte deterioration caused by the volume expansion of coked Ni anode. Therefore, the PC-SOFC performance degradation at this stage was irreversible. Normally, after long time operation in syngas, the deposited carbon atoms would develop sufficient C–C bonds and accumulate to form coke on Ni surface, which was thermodynamically unstable at high temperature. If the formed coke was not removed in time, it would tend to dissolve into and then grow inward to bulk Ni crystal lattice, resulting in serious metallic structural disintegration. This catastrophic interaction between coke and metal is known as metal dusting [22]. Since the 3rd stage poisoning always overlapped with the 2nd stage, precisely locating its starting point was not an easy task throughout the experiment. Usually, the cell performance deterioration started to become completely

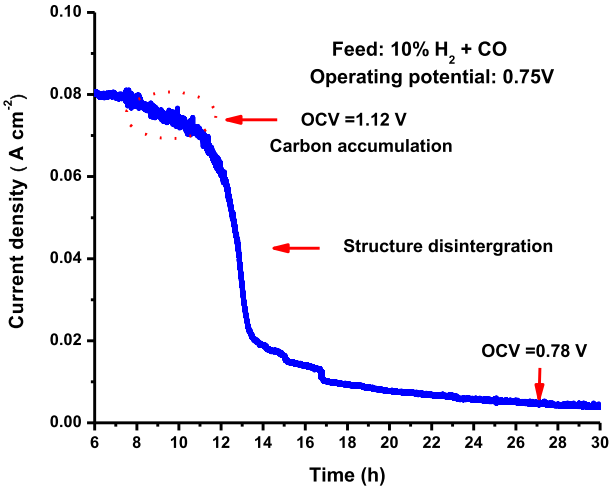

Fig. 14. Influence of carbon deposition on PC-SOFC performance under potentiostatic mode. OCV was recorded in pure H_2.

irreversible after 8 h of operation in 10% H_2 + CO. It should be noted that anode fuel flow rate could influence the 3rd stage poisoning and a higher flow rate of syngas could shorten the time of electrolyte cracking (Fig. 15).

Since CO_2 was generated via reaction (6) and water gas shift reaction, a major concern associated with the PC-SOFC stability during longevity test was the interaction between CO_2 and BZCY. This interaction could change the properties of both the anode and the electrolyte. Thus, the concentration of CO_2 in the anode chamber was measured from the anode effluent by GC. The analytical results revealed that the CO_2 concentration was below 2% under all the experimental conditions. The calculated equilibrium composition of the input feed (10% H_2 + CO) at 700 °C is shown in Fig. 16 and it also confirmed that no apparent gaseous composition change could be expected. Besides, because numerous studies have proved the good chemical stability of BZCY in the environment where the CO_2 concentration was around 10% [23–25], the slow deterioration of BZCY that led to the gradual and irreversible current drop was unlikely to occur. Thereby, the side reaction effects were unlikely to overshadow the determination of the CO poisoning effect in PC-SOFC.

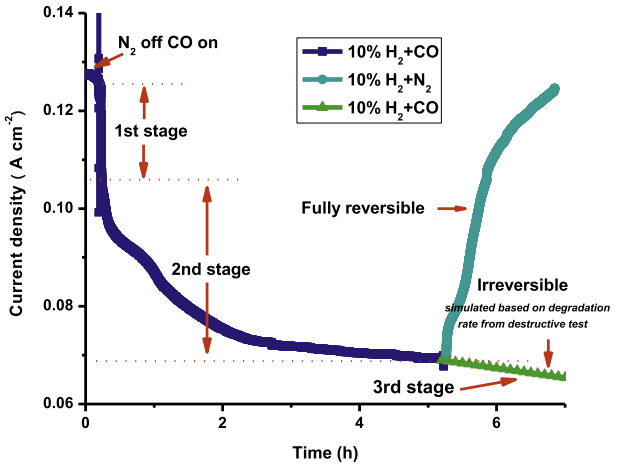

Fig. 13. An overview of three stages of CO poisoning and recovery curves in Ni based PC-SOFC.

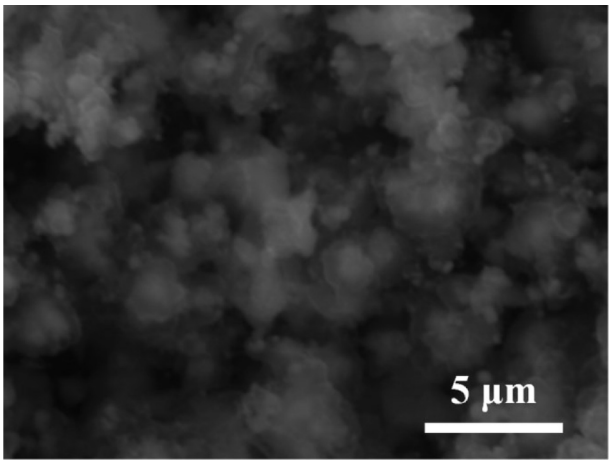

Fig. 15. Microstructure of carbon deposits on the Ni anode after prolonged PC-SOFC operation in syngas at 700 °C.

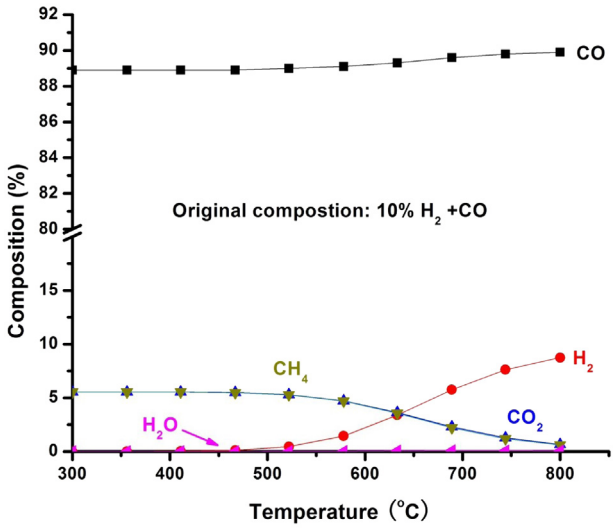

Fig. 16. Equilibrium composition of 10% H_2 + CO at various temperatures.

4. Conclusions

The mechanism of CO poisoning in PC-SOFC at high temperature was significantly different from that of the low temperature catalyst deactivation observed in PEMFC. In PC-SOFC, the initial poisoning effect was instant and reversible, which could be explained using active site blocking effect caused by CO adsorbates. The 2nd stage poisoning was also fully reversible but took relatively longer time to reach equilibrium. This stage contributed more than 75% of the total revisable fuel cell performance loss. The gradual poisoning effect was interpreted through the electrochemical reaction accelerated carbon deposition on Ni. Therefore, the subsequent H_{ad} electrochemical oxidation was strongly suppressed. The third stage poisoning effect was destructive and irreversible, which was mainly caused by Ni metal dusting and BZCY electrolyte cracking under the experimental conditions. Finally, when utilizing syngas as the fuel in PC-SOFC with a Ni anode, it is highly recommended that the percentage of H_2 in the feedstock be increased to facilitate efficient fuel conversion.

Acknowledgment

Financial support from Natural Sciences and Engineering Research Council (NSERC) of Canada Strategic Project Grant is gratefully acknowledged.

References

[1] S.D. Park, J.M. Vohs, R.J. Gorte, Nature 404 (2000) 265–267.
[2] A. Atkinson, S. Barnett, R.J. Gorte, J.T.S. Irvine, A.J. McEvoy, M. Mogensen, S.C. Singhal, J. Vohs, Nature Mater. 3 (2004) 17–27.
[3] Z.P. Shao, S.M. Haile, Nature 431 (2004) 170–173.
[4] H. Iwahara, T. Esaka, H. Uchida, N. Maeda, Solid State Ionics 3–4 (1981) 359–363.
[5] W. Jamsak, S. Assabumrungrat, P.L. Douglas, N. Laosiripojana, R. Suwanwarangkul, S. Charojrochkul, E. Croiset, Chem. Eng. J. 133 (2007) 187–194.
[6] M. Ni, D.Y.C. Leung, M.K.H. Leung, J. Power Sources 194 (2009) 1226–1227.
[7] I. Luisetto, E. Di Bartolomeo, A. DEpifanio, S. Licoccia, J. Electrochem. Soc. 158 (2011) B1368–B1372.
[8] A. Arpornwichanop, Y. Patcharavorachot, S. Assabumrungrat, Chem. Eng. Sci. 65 (2010) 581–589.
[9] H.F. Oetjen, V.M. Schmidt, U. Stimming, F. Trila, J. Electrochem. Soc. 143 (1996) 3838–3842.
[10] G.A. Camara, E.A. Ticianelli, S. Mukerjee, S.J. Lee, J. McBreen, J. Electrochem. Soc. 149 (2002) A748–A753.
[11] J.H. Wee, K.Y. Lee, J. Power Sources 157 (2006) 128–135.
[12] M.J. Kahlich, H.A. Gasteiger, R.J. Behm, J. Catal. 171 (1997) 93–105.
[13] H. Iwahara, T. Yajima, H. Ushida, Solid State Ionics 70 (1994) 267–271.
[14] K. Asano, Y. Tominaga, Y. Mugikura, T. Watanabe, Solid State Ionics 181 (2010) 236–239.
[15] Y. Jiang, A.V. Virkar, J. Electrochem. Soc. 150 (2003) A942–A951.
[16] A. Eichler, Surf. Sci. 526 (2003) 332–340.
[17] G.B. Raupp, J.A. Dumesic, J. Catal. 96 (1985) 597–612.
[18] T. Ishihara, N. Horiuchi, T. Inoue, K. Eguchi, Y. Takita, H. Arai, J. Catal. 136 (1992) 232–241.
[19] P.L. Walker, J.F. Rakszawski, G.R. Imperial, J. Phys. Chem. 63 (1959) 140–149.
[20] R.E. Williford, L.A. Chick, Surf. Sci. 547 (2003) 421–437.
[21] S.B. Adler, Chem. Rev. 104 (2004) 4791–4843.
[22] J.C.N. Paz, H.J. Grabke, Oxid. Met 39 (1993) 437–456.
[23] K.H. Ryu, S.M. Haile, Solid State Ionics 125 (1999) 355–367.
[24] K.D. Kreuer, Ann. Rev. Mater. Res. 33 (2003) 333–359.
[25] S. Barison, M. Battagliarin, T. Cavallin, L. Doubova, M. Fabrizio, C. Mortalò, S. Boldrini, L. Malavasi, R. Gerbasi, J. Mater. Chem. 18 (2008) 5120–5128.